ACS OMEGA

http://pubs.acs.org/journal/acsodf

Article

Influence of Ni Precursors on the Structure, Performance, and Carbon Deposition of Ni-Al_2O_3 Catalysts for CO Methanation

Wenlong Mo,* Xingxiang Wang, Meng Zou, Xianjin Huang, Fengyun Ma, Jianzhang Zhao, and Tiansheng Zhao

Cite This: *ACS Omega* 2021, 6, 16373−16380

Read Online

ACCESS | Metrics & More | Article Recommendations

ABSTRACT: Three Ni-Al_2O_3 catalysts were prepared, in planetary ball-milling machine, by the mechanochemical method with $Al(NO_3)_3{\cdot}9H_2O$ as the aluminum precursor, $(NH_4)_2CO_3$ as the precipitant, and $Ni(NO_3)_2{\cdot}6H_2O$, $NiCl_2{\cdot}6H_2O$, and $Ni(CH_3COO)_2{\cdot}4H_2O$ as nickel precursors (the corresponding catalysts were labeled as Ni-NO, Ni-Cl, and Ni-Ac). The prepared catalysts were characterized by X-ray diffraction (XRD), temperature-programmed reduction (H_2-TPR), and N_2 adsorption−desorption technologies, and CO methanation performance evaluation was carried out for the catalysts. Results showed that the catalyst with $Ni(NO_3)_2{\cdot}6H_2O$ as the precursor presented good Ni dispersibility and a small Ni grain size of 6.80 nm. CO conversion, CH_4 selectivity, and yield of the catalyst were as high as 78.8, 87.9, and 69.8%, respectively. Carbon deposition analysis from temperature-programmed hydrogenation (TPH) characterization showed that the H_2 consumption peak area of the three samples followed the order: Ni-NO (2886.66 au) < Ni-Cl (4389.97 au) < Ni-Ac (5721.65 au), indicating that the Ni-NO catalyst showed higher resistance to carbon deposition, which might be due to its small Ni grain size.

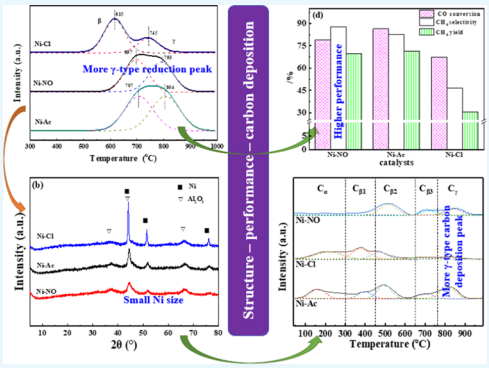

1. INTRODUCTION

With the consumption and price change of fossil fuels, the issue of energy supply has aroused widespread concern. Natural gas production from synthesis gas, the methanation process, is an effective way to alleviate the energy crisis.[1−4] CO methanation ($CO + 3H_2 \rightarrow CH_4 + H_2O$) is a typical exothermic reaction ($H_{298K} = -206.1$ kJ/mol), and some side reactions occur in the process, such as the water gas transformation reaction ($CO + H_2O \rightarrow CO_2 + H_2$) and the disproportionation reaction ($2CO \rightarrow CO_2 + C$).[5] Studies showed that the catalysts used in the CO methanation process are mainly supported catalysts, with Ni, Ru, Rh, Pt, Co, etc., as the active components,[6,7] and Al_2O_3, ZrO_2, TiO_2, SiO_2, and SiC as the support.[8−10] Among them, the Ni-Al_2O_3 catalyst shows high activity and low cost, the methanation performance of which is equivalent to that of noble-metal-based catalysts. However, there are some problems in the application of the Ni-Al_2O_3 catalyst, such as high-temperature sintering of the active component, carbon deposition on the surface of the catalyst, and catalyst poisoning.[11] Therefore, improving antisintering ability and anticoking performance of the Ni-Al_2O_3 catalyst to extend the stability of the catalyst has become a topic of concern to many researchers.

Our group used different methods to prepare Ni-Al_2O_3 catalysts and found that the mechanochemical method with planetary ball-milling machine showed many advantages in preparing industrial catalysts, including large specific surface area, high active-component dispersion, uniform particle distribution, etc. Three catalysts, Ni/Al_2O_3-J, Ni/Al_2O_3-Z, and Ni/Al_2O_3-C, were prepared by the mechanochemical one-step method, the mechanochemical-impregnation two-step method, and the impregnation method (commercial Al_2O_3 as the support). Results showed that, compared with commercial Al_2O_3, the synthesized one by the mechanochemical method presented a large specific surface area and concentrated pore size distribution. The Ni/Al_2O_3-J catalyst presented regular surface morphology and good Ni dispersibility, with CO conversion, CH_4 selectivity, and yield of 98.6, 96.0, and 94.7%, respectively, higher than that of Ni/Al_2O_3-Z and Ni/Al_2O_3-C.[12] Mo et al. also investigated the influence of ball-milling time on the structure of the Ni-Al_2O_3 catalyst via the mechanochemical one-step method. Results showed that, with a milling time of up to 60 min, the average particle size of the catalyst was small, i.e., 141 nm, with a specific surface area of 329 m^2/g, and CO conversion, CH_4 selectivity, and

Received: February 19, 2021
Accepted: May 20, 2021
Published: June 14, 2021

https://doi.org/10.1021/acsomega.1c00914
ACS Omega 2021, 6, 16373−16380

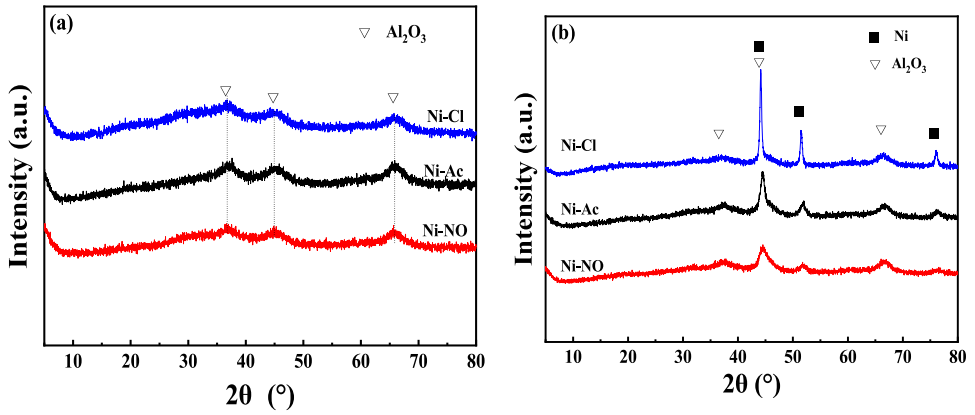

Figure 1. XRD patterns of (a) calcinated and (b) reduced catalysts.

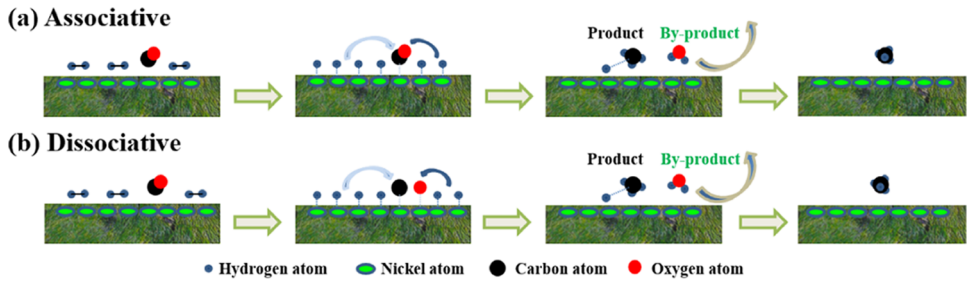

Figure 2. Catalytic reaction mechanism of CO methanation: (a) associative and (b) dissociative schemes.

Table 1. Gaussian Fitting Results from the H_2-TPR Profiles of the Catalysts

		peak areas (au)		peak area proportion (%)	
catalysts	Ni crystal size (nm)	β (500−750 °C)	γ (750−900 °C)	β (500−750 °C)	γ (750−900 °C)
Ni-Cl	15.99	5574	2367	70.19	29.81
Ni-NO	**6.80**	6250	5642	52.56	**47.44**
Ni-Ac	**7.62**	7865	7950	49.73	**50.27**

yield of 87.9, 86.8, and 74.3%, respectively. Excellent performance of the catalyst might be closely related to its small particle size (141 nm) and large specific surface area (329 m^2/g).[13] The effect of calcination temperature on the crystal structure, reduction performance, pore structure, and CO methanation performance of the Ni-Al_2O_3 catalyst was also investigated. With an increase of the calcination temperature from 350 to 700 °C, NiO was still highly dispersed on the surface of the support, while the reduction peak temperature of the catalyst was shifted to a high temperature. Among them, the cat-450 sample with a calcination temperature of 450 °C showed a higher specific surface area of 350 m^2/g and higher performance, with CO conversion, CH_4 selectivity, and yield of 97.8, 88.2, and 86.2%, respectively.[14]

In this study, three Ni-Al_2O_3 catalysts with a theoretical nickel mass fraction of 15 wt % were prepared with $Al(NO_3)_3 \cdot 9H_2O$ as the aluminum precursor, $(NH_4)_2CO_3$ as the precipitant, and $Ni(NO_3)_2 \cdot 6H_2O$, $NiCl_2 \cdot 6H_2O$, and $Ni(CH_3COO)_2 \cdot 4H_2O$ as nickel precursors. The effect of the Ni precursor on the structure, performance, and carbon deposition of the Ni-Al_2O_3 catalyst for CO methanation in slurry bed was investigated.

2. RESULTS AND DISCUSSION

2.1. Catalyst Characterization. *2.1.1. X-ray Diffraction (XRD) Analysis.* Figure 1 shows the XRD patterns of the calcinated and reduced samples. It can be seen from Figure 1a that the X-ray diffraction peaks at 2θ = 37.5, 45.5, and 67.1° are indexed to γ-Al_2O_3 species, while no characteristic peak of NiO is observed, indicating that NiO in the three catalysts is well dispersed on Al_2O_3, which is the feature of the mechanochemical one-step method.[13,15] Mo et al. prepared a series of Ni-Al_2O_3 catalysts by the method of 1,4-butynediol (BYD) hydrogenation to produce 1,4-butanediol (BED). Excellent performance of the catalyst is mainly related to the following reasons: small catalyst particle size, high Ni loading, and good Ni dispersion.[16,17] It can be seen from Figure 1b that peak positions of Al_2O_3 were not changed after the high-temperature reduction process, indicating that the spinel of Al_2O_3 remains the same, showing high stability. The existing proposed methanation mechanism can be divided into two categories:[18] (1) associative scheme (the C−O bond breaking is assisted by adatom H_{ad}) and (2) dissociative scheme (the C−O bond dissociated directly on the catalyst active sites). A schematic diagram is illustrated in Figure 2 (which does not show all of the exact intermediates for clarity). Therefore, Ni particles with high dispersibility are beneficial to give more catalytically active sites. Characteristic diffraction peaks attributed to metallic Ni appear at 2θ = 44.5, 51.8, and

https://doi.org/10.1021/acsomega.1c00914
ACS Omega 2021, 6, 16373−16380

76.4°. Among them, the shape of Ni peaks of the Ni-Cl sample is narrow and sharp, indicating a larger Ni particle size (15.99 nm, Table 1). The diffraction peak intensity of Ni-NO is smaller, with the peak shape more flatter, demonstrating that the dispersion of metallic Ni in the sample of Ni-NO is better than the other two catalysts, with a Ni crystal size of only 6.80 nm. Since the particle sizes of $Ni(NO_3)_2{\cdot}6H_2O$, $NiCl_2{\cdot}6H_2O$, and $Ni(CH_3COO)_2{\cdot}4H_2O$ are different, the dispersion of Ni on the support is diverse.[19,20] According to Scherrer's formula, the Ni crystal size of each reduced catalyst was calculated at 2θ = 51.8°, as shown in Table 1.

2.1.2. Temperature-Programmed Reduction (H_2-TPR) Analysis. Figure 3 shows the H_2-TPR profiles of the calcinated

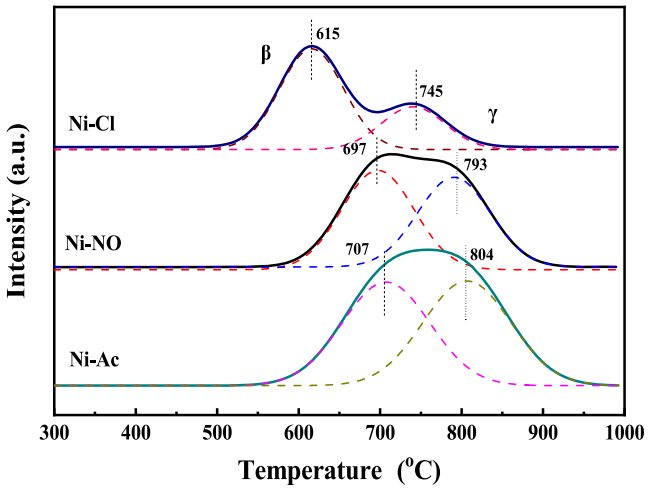

Figure 3. H_2-TPR profiles of the calcinated catalysts.

catalysts. It can be seen from the figure that the peak temperature and shape of the reduction peak of the three samples are quite different. Combining with XRD analysis, the β-type peak at 500−750 °C is not attributed to the reduction of crystal NiO, but to the reduction of amorphous NiO, which shows strong interaction with the support Al_2O_3. The reduction peak at 750−900 °C is ascribed to the γ-type peak, which usually belonged to the reduction of the $NiAl_2O_4$ spinel.[21,22] However, it can be seen from the XRD pattern that the characteristic peak of $NiAl_2O_4$ is not detected. It is speculated that the γ-type reduction peak might belong to the NiO species that entered into the Al_2O_3 crystal lattice and interacted strongly with it.

It can also be seen from Figure 3 that the reduction peak temperature of Ni-Ac and Ni-NO is higher than that of Ni-Cl, indicating that the metal−support interaction between NiO and Al_2O_3 for the former two samples is stronger than the latter one. The reduction temperature can reflect the interaction between the active component and support. The Ni-Cl sample presents lower reduction temperature, indicating that this catalyst has weak interaction between the active component and support. The Ni particles agglomerated more easily in the process of reduction, resulting in a large Ni particle size, which was not beneficial for CO methanation. And the strong interaction could effectively inhibit the migration and agglomeration of the active component at high temperatures. Table 1 shows Gaussian fitting results of H_2-TPR profiles. The β- and γ-peak area proportions of Ni-Ac and Ni-NO are nearly the same, both showing a higher proportion of the γ-type peak than Ni-Cl. From XRD results, it is speculated that the higher the area proportion of the γ-type peak, the smaller the Ni crystal size, indicating that the small Ni size of Ni-Ac and Ni-NO catalysts might probably be derived from their higher γ-type peak proportion.

2.1.3. N_2 Adsorption−Desorption Analysis. Profiles of the samples belonged to the IV-type isotherm curve and the H3-type hysteresis loop, indicating that the three samples contain many slit holes.[22] It can be seen from Figure 4b that pore size distributions of the three samples are similar, mainly located in the range of 2−15 nm, indicating that the catalysts prepared by the mechanochemical method are typical mesoporous materials.

Pore structure parameters, specific surface area, pore volume, and average pore diameter of the three calcinated samples are shown in Table 2. Usually, a high specific surface

Table 2. Pore Structure Parameters of the Catalysts

	S (m^2/g)		V (cm^3/g)		d (nm)	
catalyst	fresh catalyst	spent catalyst	fresh catalyst	spent catalyst	fresh catalyst	spent catalyst
Ni-NO	300.8	226.9	0.50	0.44	6.7	7.7
Ni-Ac	303.4	208.8	0.58	0.45	7.6	8.7
Ni-Cl	291.6	182.7	0.57	0.49	7.8	10.7

area can provide much contact surface or more active sites for reactants, which makes it possible to efficiently perform the reaction and enhance surface- or interface-related processes such as adsorption, desorption, and dissociation.[23] It can be seen from the table that, since the preparation method and

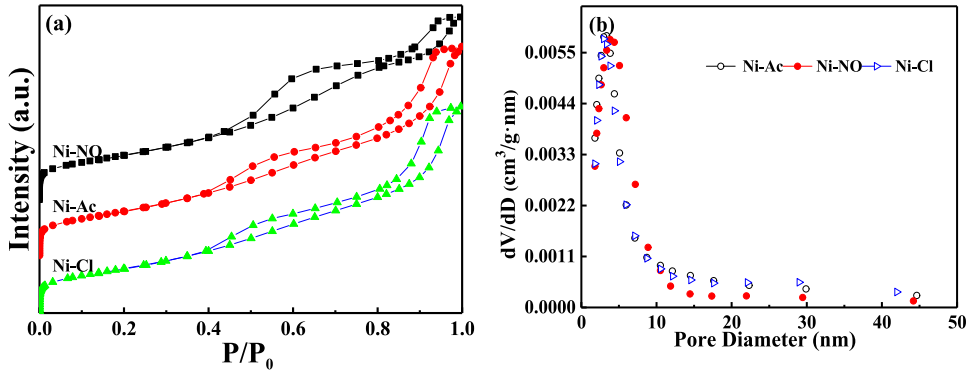

Figure 4. (a) N_2 adsorption−desorption isotherms and (b) pore size distributions of the fresh catalysts.

https://doi.org/10.1021/acsomega.1c00914
ACS Omega 2021, 6, 16373−16380

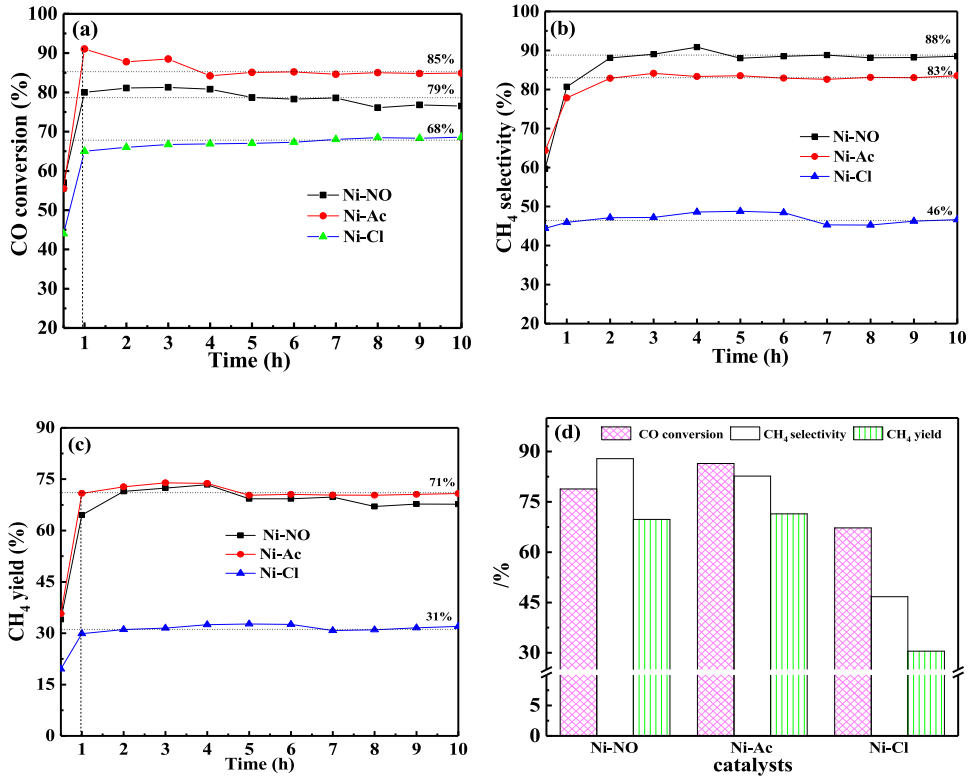

Figure 5. Evaluation results of the reduced catalysts: (a) CO conversion, (b) CH_4 selectivity, (c) CH_4 yield, and (d) activity and selectivity of the catalysts.

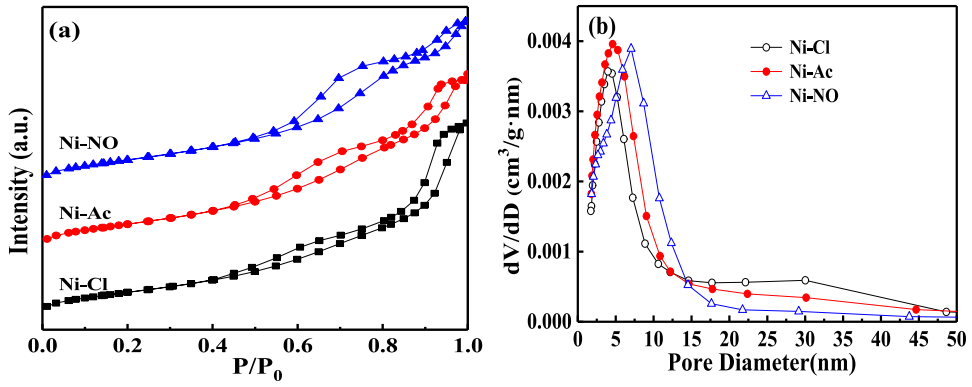

Figure 6. (a) N_2 adsorption−desorption isotherms and (b) pore size distributions of the spent catalysts.

aluminum source of each catalyst were the same, the specific surface area of the three samples is not much different, all around 300 m^2/g. In addition, the average pore diameter of Ni-NO is 6.7 nm, smaller than that of the other two catalysts (7.6−7.8 nm), which might exhibit more obvious spatial effects for small molecules.

2.2. Catalyst Performance Evaluation. Figure 5 shows the evaluation results of three reduced catalysts for CO methanation. According to Figure 5a−c, it can be seen that the catalyst activity (CO conversion) for each catalyst is unsteady before 1 h and shows a sharp upward trend, which is the induction period of catalyst activity. And the activity is nearly steady after 1 h and continues until the end of the evaluation process. Ni-Ac presents a higher CO conversion, while its CH_4 selectivity is slightly worse compared to Ni-NO. For Ni-NO, lower CO conversion and higher CH_4 selectivity can be observed, and thus the CH_4 yields of Ni-Ac and Ni-NO are almost the same. Therefore, for the Ni-Ac catalyst, it can be speculated that more byproducts would be produced. It is worth noting that, under the experimental conditions, CO can not only convert to CH_4 but also produce some byproducts such as CO_2 by the water gas shift reaction ($CO + H_2O \rightarrow CO_2 + H_2$) and small amounts of C_2H_6 and C_3H_8, which might be responsible for the lower CH_4 selectivity by Ni-Ac. In addition, X_{CO}, S_{CH_4}, and Y_{CH_4} of Ni-Cl are lower than those of the former two catalysts, which could result from its large Ni crystal size.

Time-average values of X_{CO}, S_{CH_4}, and Y_{CH_4} in steady period from Figure 5a−c are listed in Figure 5d. For CO conversion, Ni-Ac (86.4%) > Ni-NO (78.8%) > Ni-Cl (67.2%), and the order of yield of CH_4 is as follows: Ni-Ac (71.4%) > Ni-NO (69.8%) > Ni-Cl (30.5%). From the aforementioned characterizations, it can be seen that Ni dispersibility (or Ni particle size) might be responsible for the higher activity of Ni-Ac and

https://doi.org/10.1021/acsomega.1c00914
ACS Omega 2021, 6, 16373−16380

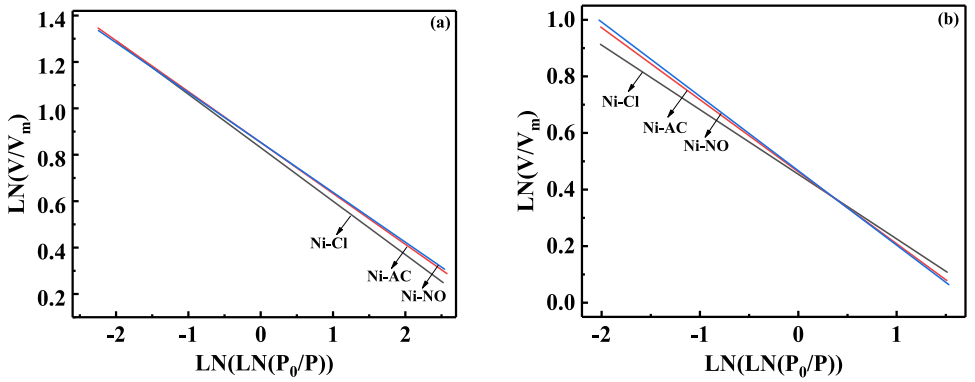

Figure 7. Linear fitting diagrams for fractal dimensions of the catalysts: (a) fresh and (b) spent catalysts.

Table 3. Fractal Dimensions and Correlation Coefficients of the Catalysts

	K		*D*		R^2	
sample	fresh catalyst	spent catalyst	fresh catalyst	spent catalyst	fresh catalyst	spent catalyst
Ni-Cl	−0.2304	−0.2284	2.3088	2.3148	0.9855	0.9863
Ni-AC	−0.2194	−0.2545	2.3418	2.2365	0.9918	0.9835
Ni-NO	−0.2149	−0.2629	2.3553	2.2113	0.9912	0.9852

Ni-NO, and the γ-type reduction peak might lead to a small Ni size, as shown in Figure 3.

2.3. Characterization of the Spent Catalyst. *2.3.1. N_2 Adsorption−Desorption Analysis.* Figure 6 shows N_2 adsorption−desorption profiles of the spent catalysts. It can be seen from Figures 6a and4a that the isotherm curves of the samples before and after the methanation reaction are similar, and they are ascribed to the IV-type isotherm. And the type of hysteresis loop of each spent catalyst is still H3, showing that the slit channel pores also exist in the materials. Pore size distribution of each spent catalyst is mainly in the range of 2−15 nm, which is not much different from the corresponding fresh one. However, the maximum dV/dD values of the three spent catalysts are lower than those of the fresh ones, indicating that the specific surface area of the spent catalyst might be decreased to some extent.

Pore structure parameters of the spent catalysts are shown in Table 2. Obvious change of pore structure parameters could be observed from Table 2. The specific surface area of Ni-NO decreased from 300.8 to 226.9 m^2/g with a decreasing rate of 24.57%, while the surface area of Ni-Ac decreased from 303.4 to 208.8 m^2/g with a decreasing rate of 31.18%, higher than that of Ni-NO. It is speculated that the decrease of surface area might be caused by carbon deposition, blocking the pore channels in catalysts. However, the pore size of Ni increased from 6.7 to 7.7 nm and that of Ni-Ac increased from 7.6 to 8.7 nm, which may be due to the collapse of micropores and the formation of macropores.

2.3.2. Fractal Dimension. Figure 7 shows linear fitting diagrams for fractal dimensions of the catalysts. The diagrams were obtained from N_2 adsorption data based on the Frenkel−Halsey−Hill (FHH) theoretical model. The fitting curves of the fresh catalysts and the spent catalysts are different, indicating that the pore structure of the Ni-Al_2O_3 catalyst has been changed after the methanation process. The fractal dimension and correlation coefficient R^2 of the catalysts are given in Table 3. The correlation coefficients R^2 of the three catalysts after calcination and after reaction are all above 0.98, demonstrating that the fitting curves presented a good linear relationship and the three catalysts were of fractal characteristics. The fractal dimension D can reflect the complexity of the channel structure, the value of which was generally between 2 and 3. The larger the value, the complex the pore structure. The fractal dimensions of the three catalysts are about 2.3, indicating that the wall surface of the pores of the Ni-Al_2O_3 catalyst prepared by the mechanical ball-milling method is smooth, which might be beneficial for methanation.

2.3.3. Temperature-programmed Hydrogenation (TPH) Analysis. Figure 8 shows the TPH profiles of the catalysts after

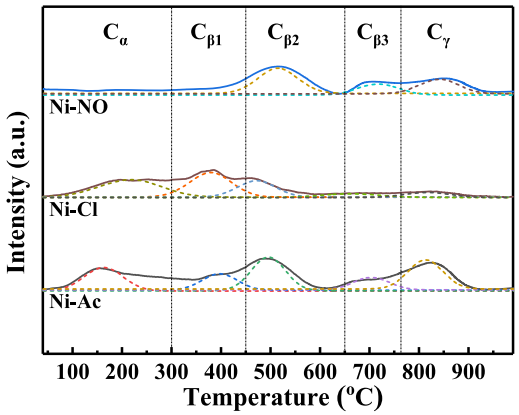

Figure 8. TPH profiles of the spent catalysts.

reaction. The H_2 consumption peak appearing before 300 °C is attributed to the hydrogenation of amorphous carbon (C_α). This kind of carbon shows high activity and is easy to be hydrogenated at a low temperature to form CH_X species; this is also the desired type of carbon deposition for carbon-related reactions. This type of carbon is easy to transform into β-type carbon species with lower activity at a high temperature, which is the intermediate species of methanation.[24−26] The peak at 300−450 °C is caused by hydrogenation of high-activity filamentous carbon ($C_{\beta1}$), and the peak ranging from 450 to 650 °C is ascribed to hydrogenation of low-activity filamentous carbon or coated carbon ($C_{\beta2}$). Furthermore, the appearance

https://doi.org/10.1021/acsomega.1c00914
ACS Omega 2021, 6, 16373−16380

of a peak at 650−750 °C may be due to the infiltration of filamentous carbon into the micropores of the catalyst, labeled as $C_{\beta 3}$, requiring a higher temperature to be hydrogenated compared with the former three types of carbon. And the H_2 consumption peak in the temperature range of 750−900 °C belonged to C_γ, which might be the hydrogenation of graphite carbon. This type of carbon shows almost no activity and is an important reason for catalyst deactivation. It can be seen from the figure that the spent Ni-Ac catalyst presented all types of carbon deposition, while there was no amorphous carbon for the spent Ni-NO sample, which might have resulted from the fact that the deposited amorphous carbon was too active to retain on the catalyst and that the carbon was easy to react with H_2 to produce the intermediate CH_X during the methanation process. Additionally, the spent Ni-Cl catalyst has almost no $C_{\beta 3}$, which may be due to its poor catalytic performance, and thus there is no accumulation of $C_{\beta 3}$ carbon to form stable graphite carbon.

Table 4 shows the TPH carbon deposition peak area and its relative proportion of each spent catalyst. The magnitude order of the peak area is as follows: Ni-NO (2886.66) < Ni-Cl (4389.97) < Ni-Ac (5721.65). Christensen et al.[27,28] prepared Ni-supported α-Al_2O_3 and γ-Al_2O_3 catalysts for steam reforming of methane. It is found that serious carbon deposition was attributed to the large Ni crystal size. Thus, small Ni particle size (6.80 nm) may be the reason for lower carbon deposition on the Ni-NO catalyst, showing higher anticoking performance. Therefore, it could be understood that severe carbon accumulation of the Ni-Cl catalyst might be derived from its larger Ni particle size. According to the peak area proportion, α- and β-type carbons on the Ni-Cl catalyst account for 97.37%, illustrating that active carbon that can be hydrogenated before 750 °C is the main deposited carbon for the catalyst.

Table 4. TPH Peak Area of the Spent Catalysts

	peak area (au)			area proportion (%)		
catalysts	Ni-NO	Ni-Ac	Ni-Cl	Ni-NO	Ni-Ac	Ni-Cl
C_α		1168.43	1387.86		20.42	31.61
$C_{\beta 1}$		819.24	1460.46		14.32	33.27
$C_{\beta 2}$	1439.47	1674.09	903.47	49.86	29.26	20.58
$C_{\beta 3}$	621.13	614.12	303.06	21.52	10.73	6.91
C_γ	826.06	1445.77	335.11	28.62	25.27	7.63
total	2886.66	5721.65	4389.97	100	100	100

In addition, CO conversion of Ni-Ac is higher than Ni-NO, while its CH_4 selectivity and yield were not significantly improved, which might result from the fact that much carbon was produced on the surface of Ni-Ac in the methanation process and that a large amount of C_γ (1445.77 au, from TPH profile) cannot be hydrogenated to give CH_4. On the other hand, the spent Ni-Ac catalyst presents much inert carbon (C_γ) at 750−900 °C, indicating that the catalyst might be more prone to deactivation due to carbon deposition as the reaction time prolonged.

3. CONCLUSIONS

Three Ni-Al_2O_3 catalysts, with $Ni(NO_3)_2{\cdot}6H_2O$, $NiCl_2{\cdot}6H_2O$, and $Ni(CH_3COO)_2{\cdot}4H_2O$ as nickel precursors, were prepared by the mechanochemical one-step method. The structure and performance of the catalysts showed that different nickel sources presented different effects on the Ni-Al_2O_3 catalyst. The catalysts with $Ni(NO_3)_2{\cdot}6H_2O$ and $Ni(CH_3COO)_2{\cdot}4H_2O$ as nickel sources showed a small Ni crystal size and high CO methanation activity. The specific surface area of the three catalysts decreased significantly, implying serious pore structure destruction. Compared to Ni-Ac, Ni-NO and Ni-Cl showed higher resistance to carbon deposition, which is probably related to its small Ni size.

4. EXPERIMENTAL SECTION

4.1. Catalyst Preparation. Three Ni-Al_2O_3 catalysts were prepared with $Al(NO_3)_3{\cdot}9H_2O$ as the aluminum precursor, $(NH_4)_2CO_3$ as the precipitant, and $Ni(NO_3)_3{\cdot}9H_2O$, $NiCl_2{\cdot}6H_2O$, and $Ni(CH_3COO)_2{\cdot}4H_2O$ as nickel precursors (99.99%, Tianjing Shengao Chemical Reagent Co., Ltd., China). Each catalyst was prepared, in planetary ball-milling machine (ND7-2L, Nanjing Laibu Instrument Co., Ltd., China), by the mechanochemical one-step method with mass ratios of large ball to small ball of 1:1 and ball to material of 2:1, and a ball-milling time of 60 min. After the ball-milling process, the obtained mixture was dried at 110 °C for 12 h, calcinated at 450 °C for 4 h, and reduced at 600 °C for 6 h, to obtain the activated Ni-based catalyst. The prepared catalysts were denoted as Ni-NO, Ni-Cl, and Ni-Ac according to the precursor used. The chemical reactions of different Ni precursors are shown in formulas 1−3. It can be seen that

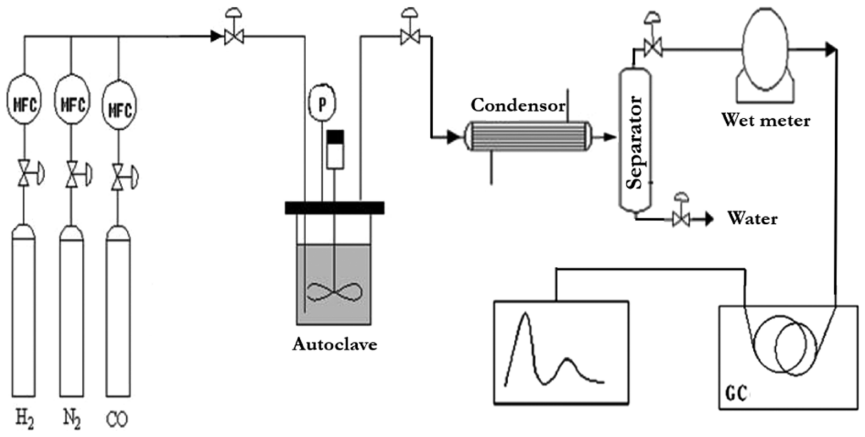

Figure 9. Schematic diagram of catalyst evaluation device.

https://doi.org/10.1021/acsomega.1c00914
ACS Omega 2021, 6, 16373−16380

$Ni(NO_3)_2{\cdot}6H_2O$, $Al(OH)_3$, corresponding salts, and CO_2 are formed in the reaction process. A homogeneous NiO/Al_2O_3 system can be formed through the calcination process of $NiCO_3$ and $Al(OH)_3$. And the Ni/Al_2O_3 catalyst with high activity might be realized after reduction

$$4Na_2CO_3 + 2Al(NO_3)_3{\cdot}9H_2O + Ni(NO_3)_2{\cdot}6H_2O = NiCO_3{\cdot}6H_2O + 2Al(OH)_3 + 8NaNO_3 + 15H_2O + 3CO_2\uparrow \quad (1)$$

$$4Na_2CO_3 + 2Al(NO_3)_3{\cdot}9H_2O + NiCl_2{\cdot}6H_2O = NiCO_3 + 2Al(OH)_3 + 6NaNO_3 + 21H_2O + 2NaCl + 3CO_2\uparrow \quad (2)$$

$$4Na_2CO_3 + 2Al(NO_3)_3{\cdot}9H_2O + Ni(CH_3COO)_2{\cdot}4H_2O = NiCO_3 + 2Al(OH)_3 + 6NaNO_3 + 19H_2O + 3CO_2\uparrow + 2Na(CH_3COO) \quad (3)$$

4.2. Catalyst Evaluation. Figure 9 shows the diagram of catalyst evaluation device. Liquid paraffin (250 mL, 99.99%, Shanghai Shanpu Chemical Co., Ltd., China) and catalyst (5 g) were put into a 500 mL reactor, with the reaction temperature of 280 °C, reaction pressure of 1.0 MPa, molar ratio of feed gases (H_2 to CO) of 3:1, gas hourly space velocity of 3000 mL/(g·h), and stirring rate of 750 r/min. And the reaction products are analyzed in situ using a GC400 gas chromatograph. A TDX201 column was used to analyze CH_4, CO_2, and unreacted CO and H_2 by a TCD detector.

CO conversion, CH_4 selectivity, and yield were used as catalyst performance indicators, which can be calculated as follows

$$X_{CO} = (V_{CO,in} - V_{out} \times y_{CO,out})/V_{CO,in} \quad (4)$$

$$Y_{CH_4} = V_{out} \times y_{CH_4,out}/(V_{CO,in} - V_{CO,out}) \quad (5)$$

$$S_{CH_4} = Y_{CH_4}/X_{CO} \quad (6)$$

where X_{CO} is the CO conversion, %; Y_{CH_4} is the CH_4 yield, %; $S_{CH_4}$is the CH_4 selectivity, %; $V_{CO,in}$ is the volume flow of CO in the feed, mL/min; V_{out} is the volume flow of product, mL/min; $y_{CH_4,out}$is the volume proportion of methane in the product mixture, %; and $y_{CO,out}$ is the volume proportion of CO in the product mixture, %.

4.3. Catalyst Characterization. *4.3.1. X-ray Diffraction (XRD).* X-ray diffraction (XRD) patterns were determined using an X-ray diffractometer (D8, Bruker Co., Ltd., Germany) with Ni-filtered Cu Ka radiation (0.15046 nm) under atmospheric pressure with 2θ from 10 to 80°.

4.3.2. Temperature-Programmed Reduction (H_2-TPR). H_2 temperature-programmed reduction and hydrogenation (H_2-TPR and TPH) profiles were obtained using a chemical adsorption instrument (TP-5080, Xianquan Industry and Trade Development Co., Ltd., Tianjin, China) from room temperature to 1000 °C with a rate of 10 °C/min.

4.3.3. N_2 Adsorption−Desorption. An Autosorb-2 physical adsorption instrument (Quantachrome Instruments) is used for N_2 adsorption−desorption characterization. N_2 is used as the adsorbate, and the adsorption−desorption measurement was carried out at liquid nitrogen temperature (−196 °C). The catalyst (0.2 g) was degassed at 110 °C for 8 h; then, the isothermal adsorption−desorption determination was performed at −196 °C. The specific surface area of the catalyst can be obtained by the Brunauer−Emmett−Teller (BET) formula, and the pore volume and pore size distribution can be obtained by the Barrett−Joyner−Halenda (BJH) formula.

4.3.4. Fractal Dimension. By analyzing the microgeometric characteristics of the catalyst, the fractal characteristics on the microscale of the pore surface can be obtained. According to experimental data of the N_2 adsorption−desorption method, the fractal dimension is calculated using the Frenkel−Halsey−Hill (FHH) model.[29] The linear expression of the FHH model is as follows

$$\ln(V/V_m) = K \ln[\ln(P_0/P)] + C$$

where V is the volume of adsorbed gas at equilibrium pressure P, cm^3/g; p_0 is the saturated vapor pressure of N_2, kPa; C is the parameter of the equation; and K is the slope of the straight line obtained by linear fitting with LN (V/V_m) as ordinate and LN $[LN(P_0/P)]$ as abscissa. When $0 > K \geq -1/3$, the relationship between fractal dimension D and slope K is as follows

$$D = 3K + 3$$

AUTHOR INFORMATION

Corresponding Author

Wenlong Mo − *State Key Laboratory of Chemistry and Utilization of Carbon Based Energy Resources and Key Laboratory of Coal Clean Conversion & Chemical Engineering Process (Xinjiang Uyghur Autonomous Region), College of Chemical Engineering, Xinjiang University, Urumqi, Xinjiang 830046, China;* orcid.org/0000-0003-3837-0915; Email: mowenlong@xju.edu.cn

Authors

Xingxiang Wang − *State Key Laboratory of Chemistry and Utilization of Carbon Based Energy Resources and Key Laboratory of Coal Clean Conversion & Chemical Engineering Process (Xinjiang Uyghur Autonomous Region), College of Chemical Engineering, Xinjiang University, Urumqi, Xinjiang 830046, China;* orcid.org/0000-0002-0076-8306

Meng Zou − *State Key Laboratory of Chemistry and Utilization of Carbon Based Energy Resources and Key Laboratory of Coal Clean Conversion & Chemical Engineering Process (Xinjiang Uyghur Autonomous Region), College of Chemical Engineering, Xinjiang University, Urumqi, Xinjiang 830046, China*

Xianjin Huang − *State Key Laboratory of Chemistry and Utilization of Carbon Based Energy Resources and Key Laboratory of Coal Clean Conversion & Chemical Engineering Process (Xinjiang Uyghur Autonomous Region), College of Chemical Engineering, Xinjiang University, Urumqi, Xinjiang 830046, China*

Fengyun Ma − *State Key Laboratory of Chemistry and Utilization of Carbon Based Energy Resources and Key Laboratory of Coal Clean Conversion & Chemical Engineering Process (Xinjiang Uyghur Autonomous Region), College of Chemical Engineering, Xinjiang University, Urumqi, Xinjiang 830046, China*

Jianzhang Zhao − *State Key Laboratory of Chemistry and Utilization of Carbon Based Energy Resources and Key*

https://doi.org/10.1021/acsomega.1c00914
ACS Omega 2021, 6, 16373−16380

Laboratory of Coal Clean Conversion & Chemical Engineering Process (Xinjiang Uyghur Autonomous Region), College of Chemical Engineering, Xinjiang University, Urumqi, Xinjiang 830046, China; State Key Laboratory of Fine Chemicals, Dalian University of Technology, Dalian, Liaoning 116024, China; orcid.org/0000-0002-5405-6398

Tiansheng Zhao − *State Key Laboratory of Chemistry and Utilization of Carbon Based Energy Resources and Key Laboratory of Coal Clean Conversion & Chemical Engineering Process (Xinjiang Uyghur Autonomous Region), College of Chemical Engineering, Xinjiang University, Urumqi, Xinjiang 830046, China; State Key Laboratory of High-Efficiency Utilization of Coal and Green Chemical Engineering, Ningxia University, Yinchuan, Ningxia 750021, China;* orcid.org/0000-0002-2292-3194

Complete contact information is available at: https://pubs.acs.org/10.1021/acsomega.1c00914

Notes

The authors declare no competing financial interest.

■ ACKNOWLEDGMENTS

The authors sincerely acknowledge the opening foundation of the State Key Laboratory of Fine Chemicals from the Dalian University of Technology (KF1904) and the foundation of the State Key Laboratory of High-Efficiency Utilization of Coal and Green Chemical Engineering (grant no. 2021-K76).

■ REFERENCES

(1) Konishcheva, M. V.; Potemkin, D. I.; Snytnikov, P. V.; Zyryanova, M. M.; Pakharukova, V. P.; Simonov, P. A.; Sobyanin, V. A. Selective CO methanation in H_2-rich stream over Ni-, Co- and Fe/CeO_2: Effect of metal and precursor nature. *Int. J. Hydrogen Energy* **2015**, *40*, 14058−14063.

(2) Liu, S.-S.; Jin, Y.-Y.; Han, Y.; Zhao, J.; Ren, J. Highly stable and coking resistant Ce promoted Ni/SiC catalyst towards high temperature CO methanation. *Fuel Process. Technol.* **2018**, *177*, 266−274.

(3) Gong, D.; Li, S.; Guo, S.; Tang, H.; Wang, H.; Liu, Y. Lanthanum and cerium co-modified Ni/SiO_2 catalyst for CO methanation from syngas. *Appl. Surf. Sci.* **2018**, *434*, 351−364.

(4) Jiménez, R.; Fuentes, K.; Paz Medina, M.; Godoy, S.; Gracia, F.; Karelouic, A. The kinetic effect of H_2O pressure on CO hydrogenation over different Rh cluster sizes. *Int. J. Hydrogen Energy* **2019**, *44*, 768−777.

(5) Jiajian, G.; Yingli, W.; Yuan, P.; Dacheng, H.; Guangwen, X.; Fangna, G.; Fabing, S. A thermodynamic analysis of methanation reactions of carbon oxides for the production of synthetic natural gas. *RSC Adv.* **2012**, *2*, 2358−2368.

(6) Eckle, S.; Denkwitz, Y.; Behm, R. J. Activity, selectivity, and adsorbed reaction intermediates/reaction side products in the selective methanation of CO in reformate gases on supported Ru catalysts. *J. Catal.* **2010**, *269*, 255−268.

(7) Zhu, H.; Razzaq, R.; Jiang, L.; Li, C. Low-temperature methanation of CO in coke oven gas using single nanosized Co_3O_4 catalysts. *Catal. Commun.* **2012**, *23*, 43−47.

(8) Liu, Q.; Wang, S.; Zhao, G.; Yang, H.; Yuan, M.; An, X.; Zhou, H.; Qiao, Y.; Tian, Y. CO_2 methanation over ordered mesoporous NiRu-doped CaO-Al_2O_3 nanocomposites with enhanced catalytic performance. *Int. J. Hydrogen Energy* **2018**, *43*, 239−250.

(9) Panagiotopoulou, P.; Kondarides, D. I.; Verykios, X. E. Mechanistic Study of the Selective Methanation of CO over Ru/TiO_2 Catalyst: Identification of Active Surface Species and Reaction Pathways. *J. Phys. Chem. C* **2011**, *115*, 1220−1230.

(10) Yongzhao, W.; Ruifang, W.; Yongxiang, Z. Effect of ZrO_2 promoter on structure and catalytic activity of the Ni/SiO_2 catalyst for CO methanation in hydrogen-rich gases. *Catal. Today* **2010**, *158*, 470−474.

(11) Kopyscinski, J.; Schildhauer, T. J.; Biollaz, S. M. A. Methanation in a fluidized bed reactor with high initial CO partial pressure: Part II-Modeling and sensitivity study. *Chem. Eng. Sci.* **2011**, *66*, 1612−1621.

(12) Zou, M.; Ma, F.; Mo, W.; Kong, L.; Liu, J.; Zhong, M.; Xiao, Y. Mechanochemical prepared Ni/Al_2O_3 catalysts and their catalytic performance for methanation. *Appl. Chem. Ind.* **2017**, *46*, 2314−2319.

(13) Mo, W.; Xiao, Y.; Ma, F.; Zhong, M.; Liu, J.; Nulahong, A. Influence of Milling Time on the Performance of Ni-Al_2O_3 Catalyst for CO Methanation Based on Slurry-bed Reactor. *J. Mol. Catal. A: Chem.* **2017**, *31*, 356−364.

(14) Mo, W.; Xiao, Y.; Ma, F.; Zhong, M.; Liu, J.; Nulahong, A. Influence of calcination conditions on the performance of Ni-Al_2O_3 catalyst for CO methanation in slurry-bed reactor. *J. Fuel Chem. Technol.* **2018**, *46*, 84−91.

(15) Gao, F.; Zou, M.; Mo, W.; Ma, F.; Liu, S.; Yang, G. Influence of precipitant on structure of Ni-Al_2O_3 catalyst and its catalytic performance in CO methanation based on slurry-bed reactor. *Mod. Chem. Ind.* **2020**, *40*, 154−162.

(16) Gao, X.; Mo, W.; Ma, F.; He, X. Effect of Ball-Milling Time on the Performance of Ni-Al_2O_3 Catalyst for 1,4-Butynediol Hydrogenation to Produce 1,4-Butenediol. *China Pet. Process. Petrochem. Technol.* **2020**, *22*, 78−86.

(17) Gao, X.; Mo, W.; Ma, F.; Fan, X. The influence of nickel loading on the structure and performance of a Ni-Al_2O_3 catalyst for the hydrogenation of 1,4-butynediol to produce 1,4-butenediol. *New J. Chem.* **2020**, *44*, 7683−7689.

(18) Miao, B.; Ma, S. S.; Wang, X.; Su, H.; Chan, S. H. Catalysis mechanisms of CO_2 and CO methanation. *Catal. Sci. Technol.* **2016**, *6*, 4048−4058.

(19) He, X.; Mo, W.; Qin, S.; Ma, F. Effect of aluminum source on the structure and performance of Ni /Al_2O_3 catalysts in CO_2-CH_4 reforming. *J. Fuel Chem. Technol.* **2020**, *48*, 221−230.

(20) Wang, X.; Zhao, B.; Jiang, D. E.; Xie, Y. Monolayer dispersion of MoO_3, NiO and their precursors on γ-Al_2O_3. *Appl. Catal., A* **1999**, *188*, 201−209.

(21) Xu, Z.; Li, Y.; Zhang, J.; Chang, L.; Duan, Z.; et al. Ultrafine NiO−La_2O_3−Al_2O_3 aerogel: a promising catalyst for CH_4/CO_2 reforming. *Appl. Catal., A* **2001**, *213*, 65−71.

(22) Chen, X.; Honda, K.; Zhang, Z. G. CO_2-CH_4 reforming over NiO/γ-Al_2O_3 in fixed-bed/ fluidized-bed switching mode. *Catal. Today* **2004**, *93*−*95*, 87−93.

(23) Wei, L.; Jun, L.; Dongyuan, Z. Mesoporous materials for energy conversion and storage devices. *Nat. Rev. Mater. Mater.* **2016**, *1*, No. 16023.

(24) Mo, W.; Ma, F.; Liu, Y.; Liu, J.; Zhong, M.; Nulahong, A. Preparation of porous Al_2O_3 by template method and its application in Ni-based catalyst for CH_4/CO_2 reforming to produce syngas. *Int. J. Hydrogen Energy* **2015**, *40*, 16147−16158.

(25) Mo, W.; Ma, F.; Ma, Y.; Fan, X. The optimization of Ni-Al_2O_3 catalyst with the addition of La_2O_3 for CO_2-CH_4 reforming to produce syngas. *Int. J. Hydrogen Energy* **2019**, *44*, 24510−24524.

(26) Mo, W.; Ma, F.; Liu, J.; Zhong, M.; Nulahong, A. A study on the carbonace ous de position on Ni-Al_2O_3 catalyst in CO_2-CH_4 reforming on the basis of te mpe rature -programmed hydroge nation characte rization. *J. Fuel Chem. Technol.* **2019**, *47*, 549−557.

(27) Christensen, K. O.; Chen, D.; Lodeng, R.; Holmen, A. Effect of supports and Ni crystal size on carbon formation and sintering during steam methane reforming. *Appl. Catal., A* **2006**, *314*, 9−22.

(28) Chen, D.; Christensen, K. O.; Ochoa-Fernandez, E.; Yu, Z. X.; Totdal, B.; Latorre, N.; Monzon, A.; Holmen, A. Synthesis of carbon nanofibers: effects of Ni crystal size during methane decomposition. *J. Catal.* **2005**, *229*, 82−96.

(29) Zhou, Q. C. Microwave-assisted preparation of Ni-W-P/γ-Al_2O_3 catalyst for coal tar hydrogenation. *Ind. Catal.* **2019**, *27*, 47−54.